ingegneria sismica
International Journal of Earthquake Engineering
Anno XLII – Num.1 - 2025

ANALYSIS OF THE EFFECT OF VISCOUS DAMPER PARAMETERS ON THE SEISMIC RESPONSE CONTROL PERFORMANCE OF HIGH-RISE BUILDINGS

Zora Goodwin
University of Alaska

SUMMARY: *Viscous dampers, as one type of energy dissipation device, have clear mechanical concepts and excellent vibration damping performance, making them the most widely used energy dissipation and vibration damping devices in current engineering applications. This paper aims to investigate the impact of setting viscous damper parameters on the seismic response control effectiveness of high-rise buildings. Through engineering examples, the Maxwell restoring force model is utilized, and the ETABS finite element analysis software is employed to establish a computational model. Using indicators such as inter-story shear force and inter-story displacement angle, the paper verifies the excellent energy dissipation and vibration damping performance of viscous dampers. The study indicates that under seismic loads, the seismic damping effect of viscous dampers on the horizontal displacement of high-rise building floors is superior to that of structural inter-story shear forces, with corresponding damping rates of 73.68% and 37.04%, respectively. Additionally, the damping coefficient significantly influences the seismic damping performance of viscous dampers, while the parameter values of the velocity index have a negligible impact on their seismic damping performance. Viscous dampers, without increasing structural stiffness, provide additional damping to effectively assist the structure in dissipating seismic input energy, thereby reducing the structure's dynamic response and achieving excellent seismic damping effects.*

KEYWORDS: Maxwell restoring force model, viscous dampers, seismic response, high-rise buildings

1 Introduction

With the development of China's economy, super-high-rise buildings have become iconic landmarks of a city. High-rise and super-high-rise buildings are characterized by their height and flexibility, making them highly sensitive to wind loads and prone to significant dynamic responses under horizontal seismic forces [1, 2, 3]. Passive energy dissipation systems both domestically and internationally primarily achieve this through the installation of viscous dampers, tuned liquid dampers (TLD), and tuned mass dampers (TMD) [4]. The principle of TMD vibration reduction involves adjusting its own vibration frequency to be near the primary vibration frequency of the structure, causing the tuned mass damper and the main structure to resonate, thereby achieving energy dissipation and vibration reduction [5, 6, 7]. TLD primarily dissipates

*drzoragoodwinjr@gmail.com

the energy generated by structural vibrations through the oscillation and viscosity of water [8]. Compared to viscous dampers, TLDs and TMDs are highly sensitive to the structure's natural frequency. Additionally, there are significant discrepancies between the theoretically calculated values and measured values of the natural frequency, as well as between different measurement methods, which can lead to deviations in the estimated vibration reduction effects [9, 10, 11, 12].

Currently, TLDs and TMDs are primarily used for wind resistance, but they have drawbacks such as large spatial requirements, higher costs for equivalent vibration reduction effects, and exacerbation of structural torsion effects [13, 14, 15]. Viscous dampers, which provide additional damping without additional stiffness, are widely applied in seismic isolation layers in high-intensity zones to reduce deformation of the isolation layer and prevent damage caused by excessive deformation [16, 17, 18, 19]. Additionally, after installing viscous dampers, the structural additional damping ratio can be flexibly adjusted to achieve the desired seismic isolation objectives, and the collaborative function between seismic isolation bearings and viscous dampers facilitates parameter optimization [20, 21, 22]. As a result, directly installing viscous dampers in building structures has become a widely accepted energy-dissipating vibration reduction method.

There has been extensive research on viscous dampers. Wolff et al. [23] conducted a response control analysis of viscous damper devices on seismic isolation structures, using low-damping rubber (LDE) and single-friction pendulum (SFP) as seismic isolation bearings. They found that linear viscous damper devices offer more benefits than drawbacks when the seismic isolation system has low displacement requirements. Ras and Boumechra [24] proposed combining steel frame structures with fluid viscous dampers (FVDs), which have the potential for passive energy dissipation without increasing structural stiffness. The effective combination of the two can provide buildings with more stable seismic response control. Tan et al. [25] designed a viscous damper structure suitable for piston-mode resonance. By establishing and improving the potential flow model, this structure can effectively capture resonance amplitude and frequency under various damping conditions. Milanchian et al. [26] demonstrated that viscous dampers, as preferred auxiliary energy dissipation devices for structural vibration control, also play a significant role in lateral displacement control strategies for buildings. By analyzing the impact of viscous damper nonlinear behavior on building vertical isolation structures, they reduced the seismic response of buildings.

Additionally, since the arrangement methods of viscous dampers have their own advantages and disadvantages, the specific selection should be made by comprehensively considering the arrangement characteristics of different structural systems. The optimal arrangement of viscous dampers not only improves the wind and seismic performance of the structure but also effectively ensures the structural functionality. De Domenico et al. [27] investigated optimization methods for the damping coefficients and layout schemes of fluid viscous dampers (FVDs). As a mature supplementary energy-dissipating device for structural seismic protection, optimizing their design methods can enhance their seismic performance. Dall'Asta et al. [28] studied the influence of engineering demand parameters and uncertainty inputs on the seismic performance of viscous dampers. They also employed harmonic analysis methods to assess the sensitivity of damper characteristic changes to seismic dynamic responses, thereby obtaining the excess probability of engineering demand parameters for buildings. Del Gobbo et al. [29] evaluated various distribution strategies for viscous dampers within buildings, aiming to identify the optimal arrangement method that improves inter-story displacement and inter-story acceleration, thereby significantly enhancing the building's seismic performance and reducing repair costs. Chen and Xiong [30] developed a foundation isolation device (FPB-VD) composed of a fric-

tion pendulum bearing and a viscous damper. Experimental results demonstrated that the device exhibits high effectiveness in reducing structural acceleration and deformation demands. Cucuzza et al. [31] established an accurate numerical model for viscous dampers, considering the variability of device production parameters. They introduced a genetic algorithm to optimize the design objective function of fluid viscous dampers, achieving high accuracy and stability. Kandemir-Mazanoglu and Mazanoglu [32] conducted a parametric study on the seismic performance of buildings, pointing out that reasonable viscous damper capacity and quantity can effectively prevent structural impacts between adjacent buildings. They proposed an optimization program based on an improved additional damping ratio equation to determine the optimal damper capacity.

This paper first provides a brief introduction to the vibration damping principles, classification, and restoring force models of viscous dampers, with the Maxwell model selected as the theoretical model for the viscous dampers in this study. Subsequently, the parameters of viscous dampers and their significance are analyzed, and the effects of these two parameters—control velocity index and damping coefficient—on the seismic response control performance of high-rise buildings are investigated through separate analyses. Furthermore, the vibration damping performance of viscous dampers is validated through engineering examples. Finally, five viscous damper layout schemes are proposed and compared with the original structure, from which the optimal scheme is selected.

2 Mechanical model and design parameters of viscous dampers

2.1 Vibration damping mechanism of viscous dampers

2.1.1 Principle of the energy method

By installing viscous dampers in the original structure to form a composite damper structure, the dampers dissipate a large amount of seismic energy through hysteretic energy dissipation under seismic loads, rapidly attenuating the seismic response of the original structure and preventing damage. The seismic isolation principle of viscous dampers can be described from an energy perspective. Under seismic loads, the energy equation of the original structure is:

$$E_{eq} = E_k + E_d + E_t + E_h, \tag{1}$$

where E_{eq} represents the energy input from seismic forces into the original structural system, E_k represents the structural kinetic energy, E_d represents the structural damping energy dissipation, E_t represents the structural elastic deformation energy, and E_h represents the structural plastic deformation energy dissipation.

In the above energy equation, the damping energy dissipation of the structural system accounts for a very small proportion of the seismic input energy and can be neglected. After the structural system completes its elastic deformation, it primarily relies on the plastic deformation of the structural system to dissipate the seismic input energy. The more seismic energy dissipated, the greater the extent of plastic deformation, and the more severe the structural damage.

Energy dissipation and seismic isolation structural vibration energy equation:

$$E_{eq} = E_k + E_d + E_t + E_c + E_h, \tag{2}$$

where, E_c represents the seismic energy consumed by the energy dissipation and vibration reduction device.

From the above energy Eq. (2), it can be seen that the viscous damper enters the working state before the original structure undergoes plastic deformation and consumes the input seismic energy in the form of additional damping energy dissipation E_c, significantly attenuating the energy dissipation of the original structure's plastic deformation, thereby achieving the goal of controlling the structural seismic response and reducing the degree of damage to the original structure.

2.1.2 Vibration damping principle of viscous dampers

Viscoelastic dampers dissipate seismic input energy through additional damping energy dissipation. Damping is the fundamental cause of structural vibration attenuation. Installing viscoelastic dampers effectively increases the damping ratio of the original structure. The principle of seismic energy dissipation by viscoelastic dampers can be explained using the theory of single-mass forced vibration analysis. Let M represent the dynamic amplification factor. The vibration response of the mass can be understood as equal to the structural dynamic amplification factor M multiplied by the structural static response. Therefore, the magnitude of M determines the intensity of the structural system's vibration response. The formula for calculating M is related to the structural natural frequency and structural damping ratio. Generally, the damping ratio of building structures cannot reach 0.7, so the structural vibration response exhibits an "amplification" effect. Typically, the damping ratio of concrete structures is 0.05, so under seismic loads, the structural vibration response exhibits an "amplification" effect, which is detrimental to the structural seismic performance. Installing viscous dampers can increase the structural damping ratio, and the M value decreases as the structural damping ratio increases, thereby causing the structural vibration response to exhibit a "damping" effect.

The vibration damping mechanism of viscous dampers utilizes the viscous damping force generated by the interaction between the viscous damping material and internal components to dissipate seismic energy through hysteresis. A viscous damper typically consists of a cylinder, piston, viscous fluid damping material, and a moving guide rod. The piston is equipped with damping holes. When the piston moves back and forth within the cylinder, the hydraulic pressure difference causes the viscous fluid to flow through the throttle holes, generating viscous resistance to achieve energy dissipation and vibration reduction.

2.2 Classification of viscous dampers

A viscous damper is a velocity-dependent damper. Based on different construction principles, it can be classified into cylinder-type viscous fluid dampers, viscous damping walls, and barrel-type viscous fluid dampers. This paper analyzes and studies cylinder-type viscous fluid dampers.

2.2.1 Cylinder-type viscous fluid damper

Cylinder-type viscous fluid dampers consist of a cylinder body, guide rod, piston, and viscous fluid material. Based on the different structural forms of the piston, they can be classified into porous-type, gap-type, and hybrid-type viscous dampers. The structural forms of the porous-type and gap-type dampers are shown in Figures 1 and 2, respectively. Based on the guide rod design, they can be further classified into single-rod viscous dampers and double-rod viscous dampers, with their internal structures shown in Figures 3 and 4, respectively.

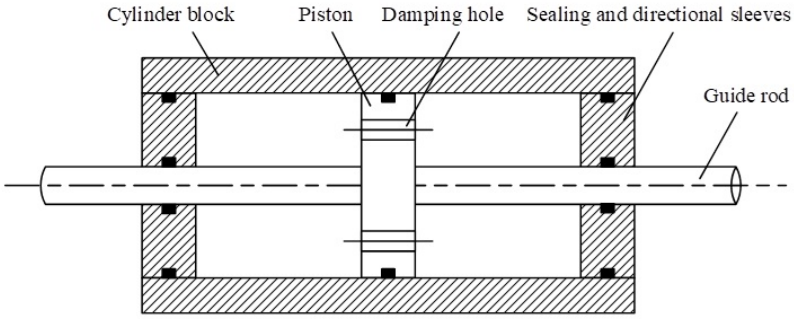

Figure 1: Porous viscous fluid damper

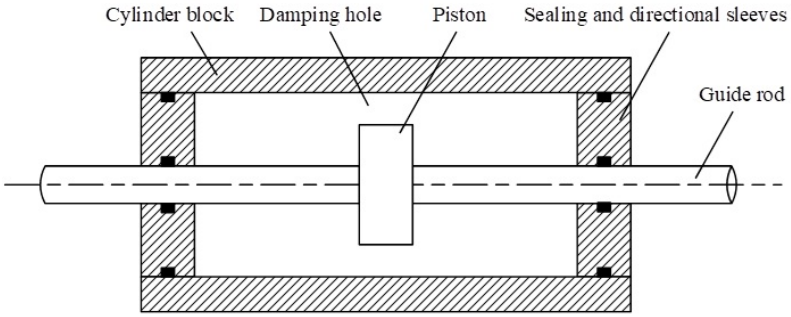

Figure 2: Intermittent viscous fluid damper

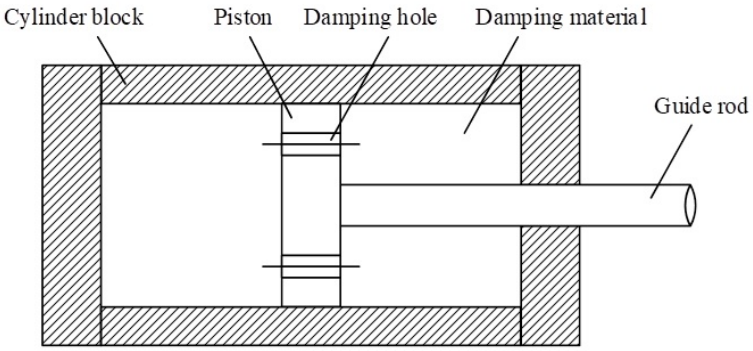

Figure 3: Single-rod type viscous damper

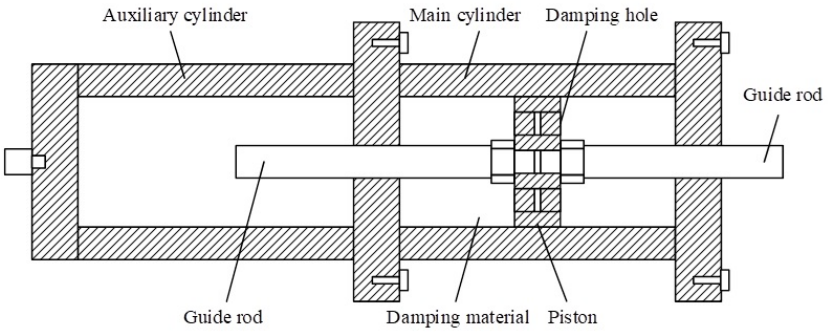

Figure 4: Double-rod type viscous damper

1. A porous viscous fluid damper seals the gap between the closed piston and the inner wall of the cylinder, with a certain number of damping holes designed on the piston. When the piston moves within the cylinder, the hydraulic pressure difference causes the viscous fluid material to flow through the damping holes, generating viscous resistance to achieve the damper's design objective.

2. Gap-type viscous fluid dampers have a gap between the piston and the inner wall of the cylinder. When the piston moves relative to the cylinder, the viscous fluid material passing through the gap generates frictional resistance, which is used to dissipate the energy input from earthquakes. However, because it is difficult to precisely control the damping force provided, the development and application of gap-type viscous fluid dampers are limited.

3. Single-rod viscous damper: When the guide rod moves back and forth inside the cylinder body, the fluid hydraulic difference causes the viscous damping material to flow inside the cylinder and pass through the damping holes, forming a viscous damping force that consumes the input seismic energy. However, single-rod viscous dampers are prone to "locking" or "cavity" phenomena, causing the damper guide rod to stop moving back and forth and the damper to fail.

4. Double-rod viscous damper: Single-rod viscous dampers have certain drawbacks, so research and development efforts led to the creation of double-rod viscous dampers. This type of viscous damper has a main cylinder and an auxiliary cylinder connected by a guide rod, so that the volume of the main cylinder does not change during the reciprocating motion of the guide rod, thereby avoiding the shortcomings of single-rod viscous dampers. This type of viscous damper has a simple structural design, excellent sealing performance, and rarely fails. It is also easy to install and maintain, making it widely used in practical engineering applications.

2.2.2 Viscous damping wall

The structural configuration of the viscous damping wall is shown in Figure 5, consisting of an inner steel plate, an outer steel plate, and viscous fluid. The inner steel plate is fixed to the upper floor during installation, while the outer steel plate is fixed to the lower floor. When external loads act on the structure, relative displacement occurs between the upper and lower floors, causing the inner steel plate to disturb the viscous damping material and generate hysteretic energy dissipation, thereby consuming the seismic energy absorbed by the structure. Viscous damping walls exhibit significant seismic isolation effects but are relatively expensive, resulting in limited application in actual engineering projects.

2.3 Restoring force model of viscous dampers

The restoring force models of viscous dampers mainly include linear models, Maxwell models, Kelvin models, fractional derivative models, etc. Below is a brief introduction to the most commonly used ones.

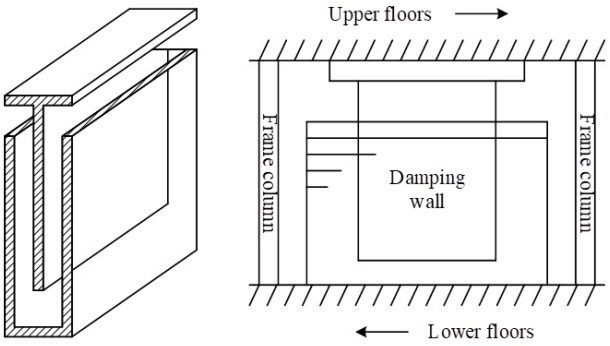

Figure 5: Structural of viscous damping wall

2.3.1 Linear Models

In a linear model, the speed determines the output of the damper, and the damping force $F_d(t)$ can be expressed by the following equation:

$$F_d(t) = C\dot{u}(t), \tag{3}$$

where, C is the damping coefficient of the linear viscous damper, and $\dot{u}(t)$ is the movement speed.

If a sinusoidal harmonic wave acts on a linear viscous damper, that is:

$$u(t) = u_0 \sin(\omega t), \tag{4}$$

where, u_0, ω, t represents the wave amplitude, frequency, and time, respectively.

Substituting (4) into (3) yields the damping force:

$$F_d(t) = Cu_0\omega\cos(\omega t). \tag{5}$$

From Eqs. (4) and (5), we obtain:

$$\left(\frac{F_d}{Cu_0\omega}\right)^2 + \left(\frac{u}{u_0}\right)^2 = 1. \tag{6}$$

It can be seen that the force-displacement relationship curve of a linear damper is elliptical. The energy consumed by the damper during one cycle is:

$$W_d = \pi C\omega u_0^2. \tag{7}$$

2.3.2 Kelvin model

The medium stiffness of the Kelvin model [33] determines the properties of linear viscous dampers. When a sinusoidal harmonic wave acts on the damper, the damping force is expressed as

$$F_d(t) = k\,u(t) + C\,\dot{u}(t) = F_0\,\sin(\omega t + \phi), \tag{8}$$

where C is the damping coefficient, k is the storage stiffness, F_0 is the amplitude of the damping force, and ϕ is the phase difference between displacement and damping force.

From Eqs. (4) and (8), it follows that

$$\left(\frac{F_d - ku}{Cu_0\omega}\right)^2 + \left(\frac{u}{u_0}\right)^2 = 1, \tag{9}$$

which is equivalent to

$$\left(\frac{F_d}{Cu_0\omega}\right)^2 + \left(\frac{u}{u_0}\right)^2 \left[1 + \left(\frac{k}{C\omega}\right)^2 - 2\left(\frac{k}{C\omega}\right)\left(\frac{F_d}{Cu_0\omega}\right)\left(\frac{u_0}{u}\right)\right] = 1. \tag{10}$$

The damping coefficient of the damper is given by

$$C = \frac{W_d}{\pi\omega u_0^2}. \tag{11}$$

The energy storage stiffness of the damper is determined as

$$k = \frac{F_0}{u_0}\left[1 - \left(\frac{Cu_0\omega}{F_0}\right)^2\right]^{1/2}. \tag{12}$$

The phase difference between displacement and damping force is expressed as

$$\phi = \arcsin\left(\frac{Cu_0\omega}{F_0}\right). \tag{13}$$

Since most viscous dampers exhibit frequency dependence, the expression for the complex Kelvin model damping force can be obtained through Fourier transformation and Euler's formula:

$$F_d(\omega) = k(\omega)\,u(\omega) + i\omega C(\omega)\,u(\omega), \tag{14}$$

or equivalently,

$$F(\omega) = [k_1(\omega) + ik_2(\omega)]\,u(\omega) = k^*(\omega)\,u(\omega), \tag{15}$$

where the composite stiffness $k^*(\omega)$ is defined as

$$k^*(\omega) = k_1(\omega) + ik_2(\omega). \tag{16}$$

Here, the loss stiffness $k_2(\omega)$ is calculated from

$$k_2(\omega) = \omega C(\omega). \tag{17}$$

2.3.3 Maxwell's model

When the frequency dependence of the viscous damper is relatively strong, a more accurate representation can be obtained using the "damper–stiffness continuity model" of the Maxwell model [34], in which the "spring unit" and the damper unit are connected in series.

Let the displacements of the "spring unit" and the damping unit be $u_1(t)$ and $u_2(t)$, respectively. Then,

$$u_1(t) = u_2(t) = u(t), \tag{18}$$

$$k\,u_1(t) = C_0\,\dot{u}_2(t) = F_d(t). \tag{19}$$

Combining the above two relations, we obtain

$$F_d(t) + \lambda \dot{F}_d(t) = C_0 \dot{u}(t), \tag{20}$$

where C_0 denotes the linear damping coefficient at zero frequency, $F_d(t)$ is the damping force, k is the stiffness coefficient in the "infinite" frequency domain, and λ is the relaxation time coefficient, given by $\lambda = C_0/k$.

Eq. (20) can be rewritten as

$$\dot{F}_d(t) = f(F,u,\dot{u},t) = -\frac{1}{\lambda}F_d(t) + \frac{C_0}{\lambda}\dot{u}(t). \tag{21}$$

In structural nonlinear analysis, Eq. (21) is solved simultaneously with the equations of motion of other structural components.

By applying a Fourier transform together with Euler's formula, the expression for the complex Maxwell model is obtained as

$$u(\omega) = u_1(\omega) = u_2(\omega), \tag{22}$$

$$k^*(\omega)u(\omega) = k\,u_1(\omega) = iC_0\omega\,u_2(\omega). \tag{23}$$

Combining Eqs. (22) and (23), we obtain

$$k^*(\omega) = k\frac{iC_0\omega}{k + iC_0\omega} = \frac{ik^2C_0\omega + kC_0^2\omega^2}{k^2 + C_0^2\omega^2}, \tag{24}$$

or equivalently,

$$k^*(\omega) = \frac{(C_0^2\omega^2/k) + iC_0\omega}{1 + \lambda^2\omega^2} = \frac{C_0\lambda\,\omega^2}{1 + \lambda^2\omega^2} + i\frac{C_0\omega}{1 + \lambda^2\omega^2}. \tag{25}$$

Substituting $\lambda = C_0/k$ into Eq. (25), the energy storage stiffness and loss stiffness are obtained as

$$k_1(\omega) = \frac{C_0\lambda\,\omega^2}{1 + \lambda^2\omega^2} = \frac{k\lambda^2\omega^2}{1 + \lambda^2\omega^2}, \tag{26}$$

$$k_2(\omega) = \frac{C_0\omega}{1 + \lambda^2\omega^2}. \tag{27}$$

Furthermore, the damping coefficient is given by

$$C(\omega) = \frac{k_2(\omega)}{\omega} = \frac{C_0}{1 + \lambda^2\omega^2}. \tag{28}$$

2.3.4 Wiechert model

If the viscous fluid inside the damper contains asphalt-like material with viscoelastic solid characteristics, the fluid exhibits thickening behavior under low-frequency loads. In this case, combining the Maxwell model with the Kelvin model yields the Wiechert model [35], where k_g and k_e denote the smooth stiffness and the elastic stiffness, respectively.

Let the displacements of the spring unit and damping unit in the upper branch be u_{1k} and u_{1c}, respectively, so that the total displacement of the upper branch is $u_1 = u_{1k} + u_{1c}$. The displacement of the spring unit in the lower branch is denoted as u_2. Then, the force–displacement relationships between the components of the Wiechert model can be written as:

$$\begin{cases} k u_{1k} = C_0 \dot{u}_{1c}, \\ u_{1k} + u_{1c} = u_1 = u_2 = u, \\ k_e u_2 + k u_{1k} = k_e u_2 + C_0 \dot{u}_{1c} = F_d(t). \end{cases} \tag{29}$$

From the above, it follows that:

$$\begin{cases} -\dfrac{\dot{F}_d(t)}{k} + \dfrac{k_e + k}{k} \dot{u} = \dot{u}_{1c} = \dfrac{F_d(t) - k_e u}{C_0}, \\ -\dot{F}_d(t) + k_g \dot{u} = \dfrac{1}{\lambda} [F_d(t) - k_e u], \\ F_d(t) + \lambda \dot{F}_d(t) = \lambda k_g \dot{u} + k_e u, \end{cases} \tag{30}$$

where $\lambda = C_0/k$ is the relaxation time coefficient.

Applying the Fourier transform together with Euler's formula gives the complex expression of the Wiechert model. Since the upper branch corresponds to the Maxwell model, its complex stiffness is

$$k^*(\omega)_{\text{up}} = \frac{k\lambda^2\omega^2}{1+\lambda^2\omega^2} + i\frac{C_0\omega}{1+\lambda^2\omega^2}. \tag{31}$$

The lower branch contributes purely elastic stiffness:

$$k^*(\omega)_{\text{lower}} = k_e. \tag{32}$$

Thus, for the full Wiechert model consisting of both branches, the complex stiffness can be expressed in a form analogous to the Kelvin model:

$$k^*(\omega)u = k^*(\omega)_{\text{up}}\, u_1 + k^*(\omega)_{\text{lower}}\, u_2. \tag{33}$$

Also, the displacement compatibility condition holds:

$$u_{1k} + u_{1c} = u_1 = u_2 = u. \tag{34}$$

Combining Eqs. (33) and (34) gives

$$k^*(\omega) = k_e + \frac{k\lambda^2\omega^2}{1+\lambda^2\omega^2} + i\frac{C_0\omega}{1+\lambda^2\omega^2} = k_1(\omega) + ik_2(\omega). \tag{35}$$

Therefore, the storage stiffness and loss stiffness are respectively:

$$\begin{cases} k_1(\omega) = k_e + \dfrac{k\lambda^2\omega^2}{1+\lambda^2\omega^2}, \\ k_2(\omega) = \dfrac{C_0\omega}{1+\lambda^2\omega^2}. \end{cases} \tag{36}$$

Finally, the frequency-dependent damping coefficient of the damper is obtained as

$$C(\omega) = \frac{k_2(\omega)}{\omega} = \frac{C_0}{1+\lambda^2\omega^2}. \tag{37}$$

2.3.5 Mechanical model used in this paper

In this study, a nonlinear connection element referred to as a damper is employed to simulate a viscous damper. The damping characteristics are represented using the refined Maxwell model, which comprises a series arrangement of nonlinear elements and springs. This model captures both nonlinear and linear properties, and within the software, damping elements can be assigned across multiple degrees of freedom. When conducting linear analysis of a structure, the software applies the linear properties of the element; when performing nonlinear analysis, it applies the nonlinear properties of the element. In this work, the theoretical model adopted for the viscous damper is the Maxwell model, whose nonlinear force–deformation relationship is expressed as:

$$F_d(t) = C|\dot{u}(t)|^{\alpha} = Ku_2(t), \tag{38}$$

where K denotes the spring stiffness, C is the damping coefficient of the damper, and α is the damping index. The damping index α is always positive and typically lies within the range of 0.2 to 2.0.

2.4 Parameters of viscous dampers and their determination

2.4.1 Speed index

Depending on the value of α, viscous dampers can be classified into three categories: when $\alpha > 1$, it is a super-linear viscous damper; when $\alpha = 1$, it is a linear viscous damper; and when $\alpha < 1$, it is a non-linear viscous damper. In engineering applications, the velocity exponent α of viscous dampers is generally between 0.3 and 1. When α varies, the relationship curve between the damper's output force and velocity is shown in Figure 6.

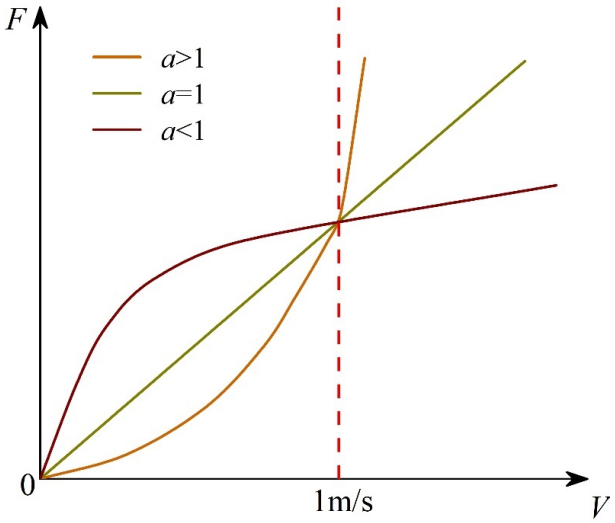

Figure 6: Force–velocity curves of viscous dampers with different velocity indices

It can be seen that nonlinear viscous dampers can generate large damping forces at lower relative speeds, while at higher relative speeds, the increase in damping force is relatively slow. Linear dampers produce much smaller damping forces than nonlinear dampers when the relative speed is less than 1 m/s, but when the relative speed exceeds 1 m/s, their damping forces are significantly greater than those of nonlinear dampers.

In most cases, the relative velocity between the two ends of a viscous damper in practical engineering applications is less than 1 m/s. Therefore, in general engineering practice, the smaller the velocity exponent α, the greater the output force of the viscous damper, and the stronger its energy dissipation capability.

2.4.2 Damping coefficient

The damping coefficient C of the viscous damper is also a parameter that must be determined. In principle, C is obtained through testing. Once the velocity index and damping coefficient are specified, the output of the damper can be calculated. When the damper output remains constant, the damping coefficient increases with α when the relative velocity $\dot{u}_D < 1$ m/s at both ends of the viscous damper. When $\dot{u}_D > 1$ m/s, the damping coefficient decreases with α.

At $\alpha = 1$, the damper is a linear viscous damper, with a damping coefficient denoted as C_L. At $\alpha < 1$, the damper is a nonlinear viscous damper, with a damping coefficient denoted as C_{NL}. Between C_{NL} and C_L, equivalent conversion can be performed based on the principle of equal damper output or equal energy dissipation.

2.4.3 Maximum output

The maximum output force is one of the key performance indicators of a viscous damper. The greater the maximum output force, the larger the size and mass of the damper itself, and the higher the corresponding manufacturing costs. At the same time, an excessively large or excessively small maximum output force can adversely affect the structural control performance.

Therefore, in practical engineering applications, the maximum output F_D is one of the necessary conditions for selecting a viscous damper. As expressed in $F = Cv^{\alpha}$, once the damping coefficient C and the velocity index α are chosen, the maximum relative velocity v between the two ends of the damper can be estimated, and then F_D can be calculated. Conversely, if the viscous damper F_D is specified first, its damping coefficient can also be readily determined using the same relationship.

2.4.4 Maximum travel

The maximum stroke of the viscous damper is also a key parameter that must be provided to the manufacturer. The maximum stroke of the damper ΔU_{DMAX} can be calculated using the following formula:

$$\Delta U_{DMAX} = f \cdot \Delta U_P, \tag{39}$$

where f is the amplification factor, and ΔU_P is the maximum elastic–plastic inter-story displacement at the floor where the damper is located. The limit values for the elastic–plastic displacement angle of structural floors can be obtained from the Building Seismic Design Code. Generally, the limit values for the elastic–plastic displacement angle of multi-story and high-rise steel structures are $\theta_P = 1/50$, and those for energy-dissipating and vibration-reducing structures are $\theta_P = 1/80$. Substituting these values into Eq. (39) yields the maximum stroke of the viscous damper $\pm|\Delta U_{DMAX}|$.

In practical engineering applications, installation errors are inevitable. Therefore, the actual maximum stroke of the damper is typically smaller than the calculated value obtained from time-history analysis. To address this, the calculated value should be multiplied by a safety factor greater than 1, based on experience, while ensuring that this value is not less than the maximum stroke corresponding to $\Delta U_P = h/80$.

3 The effect of viscous damper parameters on seismic response control performance

This section investigates the influence of viscous damper parameters on the seismic response control performance of high-rise buildings based on the mechanical model of viscous dampers.

The seismic response control performance of high-rise buildings is closely related to the selection of viscous damper parameters. In current research, the primary objective is to effectively limit floor seismic displacement and improve the seismic internal forces of load-bearing components. Therefore, the maximum horizontal displacement of floors and inter-story shear forces in the structure are selected as the research objects to investigate the influence of key performance parameters of viscous dampers on the seismic response control effectiveness in high-rise buildings. Two analysis scenarios are set: Scenario A, without dampers; Scenario B, with 50 longitudinal viscous dampers installed between floors and structural layers. Based on previous engineering design experience, Scenario B employs the following two parameter combinations for computational analysis.

Series I: Under a velocity index of $\alpha = 0.4$, the damping coefficient C_d is set to $1000, 2000, \ldots, 9000\,\mathrm{kN}\cdot(\mathrm{m}\cdot\mathrm{s}^{-1})^{-0.5}$ to examine the effect of the damping coefficient C on the vibration control effect of the viscous damper.

Series II: With $C = 3\times10^3\,\mathrm{kN}\cdot(\mathrm{m}\cdot\mathrm{s}^{-1})^{-\alpha}$, the value of α is taken as $0.1, 0.2, \ldots, 0.9$ to examine the effect of the velocity index α on seismic response control performance. To facilitate the description of damper control performance, the following damping rate is defined for comparative analysis:

$$\beta = \frac{E_{none} - E_{damper}}{E_{none}} \times 100\%, \tag{40}$$

where β represents the damping ratio, and E_{none} and E_{damper} represent the seismic response of the structural system without and with dampers, respectively.

3.1 Parameter combination series I

The results showing the effect of different damping coefficients on the seismic response control performance of critical structural components in high-rise buildings are presented in Figure 7. The shaded areas represent the standard deviation of the seismic reduction rate, indicating the degree of dispersion between the calculation results of the nine seismic waves and their average values. The same convention applies to subsequent figures.

Installing viscous dampers between floors in high-rise buildings not only effectively controls floor seismic displacement but also improves the stress conditions of structural layers. However, the impact of different damping coefficients on the maximum horizontal displacement of floors and the damping effect on structural layer shear forces varies significantly. As shown in the figure, both the maximum floor displacement damping rate and the shear damping rate generally increase monotonically with increasing damping coefficient. Under various damper parameters, the maximum damping rate for floor horizontal displacement reaches 73.68%, while the maximum shear damping rate is only 37.04%. The displacement damping rate is therefore significantly higher than the shear damping rate, indicating that viscous dampers are more effective in reducing floor horizontal displacement than in reducing structural layer shear, and that the damping coefficient plays a critical role in determining damper performance.

Taking the Northridge earthquake wave as an example, Figure 8 compares the energy dissipation curves of viscous dampers under different damping coefficients. Subfigures (a)–(c) repre-

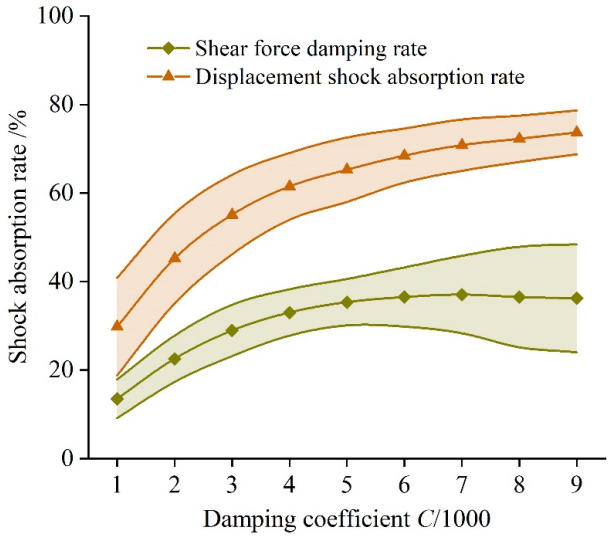

Figure 7: Influence of damping coefficient on the seismic control effect of key structural components

sent the energy dissipation of viscous dampers with damping coefficients of $1000, 2000, \ldots, 9000\,\mathrm{kN} \cdot (\mathrm{m} \cdot \mathrm{s}^{-1})^{-0.5}$, respectively. The area enclosed by the hysteresis loop represents the seismic energy dissipated by the viscous damper. It can be observed that as the damping coefficient increases, the enclosed area also increases, indicating enhanced hysteretic energy dissipation capability. This demonstrates that the damping coefficient is a decisive factor in improving the seismic energy dissipation performance of viscous dampers.

3.2 Parameter combination series II

The results of the impact of different velocity indices on the seismic response control effectiveness of critical components in high-rise buildings are shown in Figure 9. Under various velocity index conditions, the floor displacement damping ratio is significantly higher than the structural layer shear damping ratio. This indicates that installing viscous dampers between floors and structural layers can more effectively control the maximum seismic displacement of floors, while the control effectiveness on structural layer internal forces is secondary. Additionally, as the velocity index varies, the changes in floor displacement and structural layer shear damping ratios are not significant. For example, in structural layer shear, the maximum and minimum damping ratios are 35.13% and 27.57%, respectively, with a difference of only 7.56%, indicating that the parameter values of the velocity index have a very small impact on the damping effectiveness of viscous dampers.

Taking the Northridge earthquake wave as an example, the comparison of energy dissipation curves of viscous dampers under different velocity index conditions is shown in Figure 10. (a) to (c) represent the energy dissipation performance of viscous dampers when the velocity index is set to $0.1, 0.2, \ldots, 0.9$. Observation shows that as the velocity index increases, the areas enclosed by the energy dissipation curves under corresponding conditions remain largely unchanged, indicating that the parameter values of the velocity index have a negligible impact on the area of the hysteresis loop. Therefore, from the perspective of the energy dissipation principle of viscous dampers, it is evident that the influence of the velocity index on the energy dissipation capacity of viscous dampers is extremely limited.

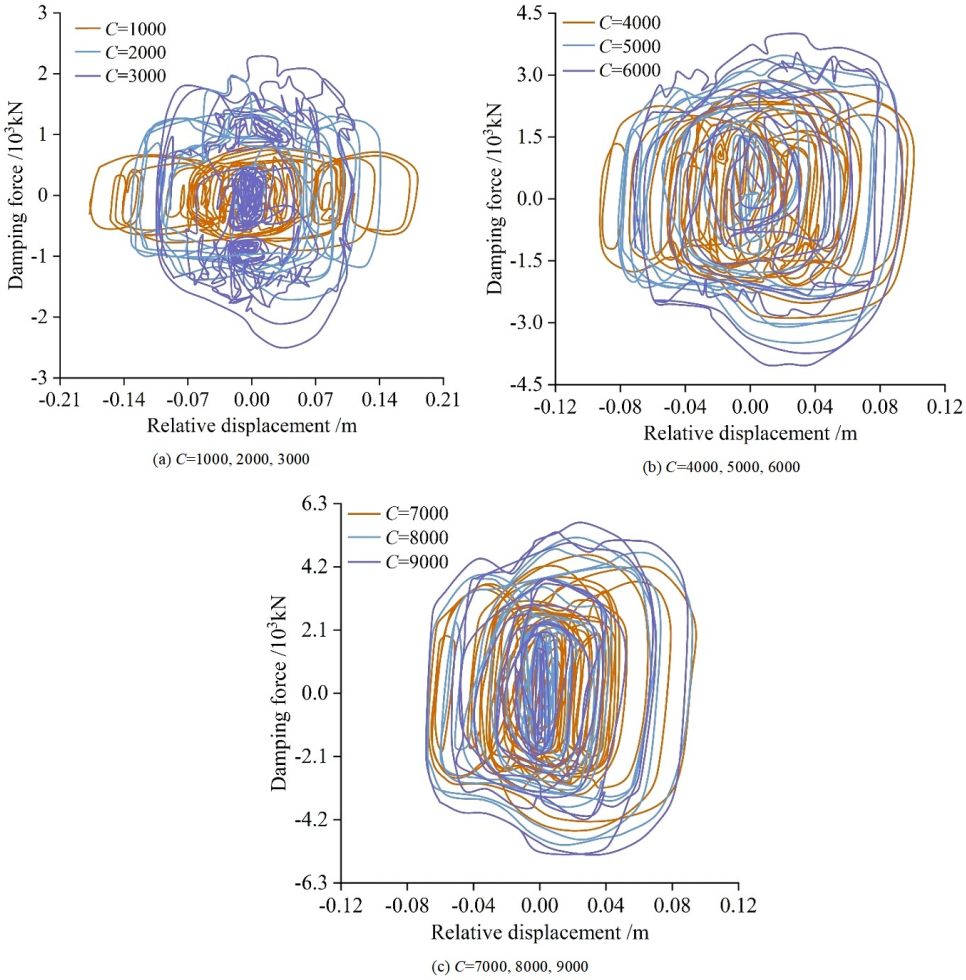

Figure 8: Energy dissipation curves of dampers under different damping coefficients

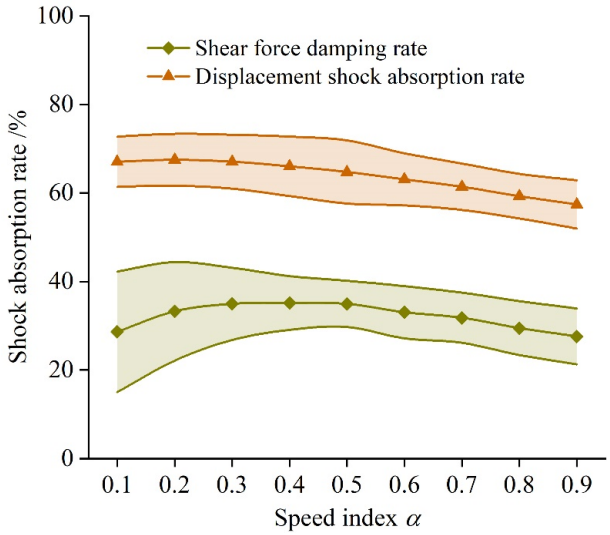

Figure 9: The influence of speed index on the shock absorption effect of key parts

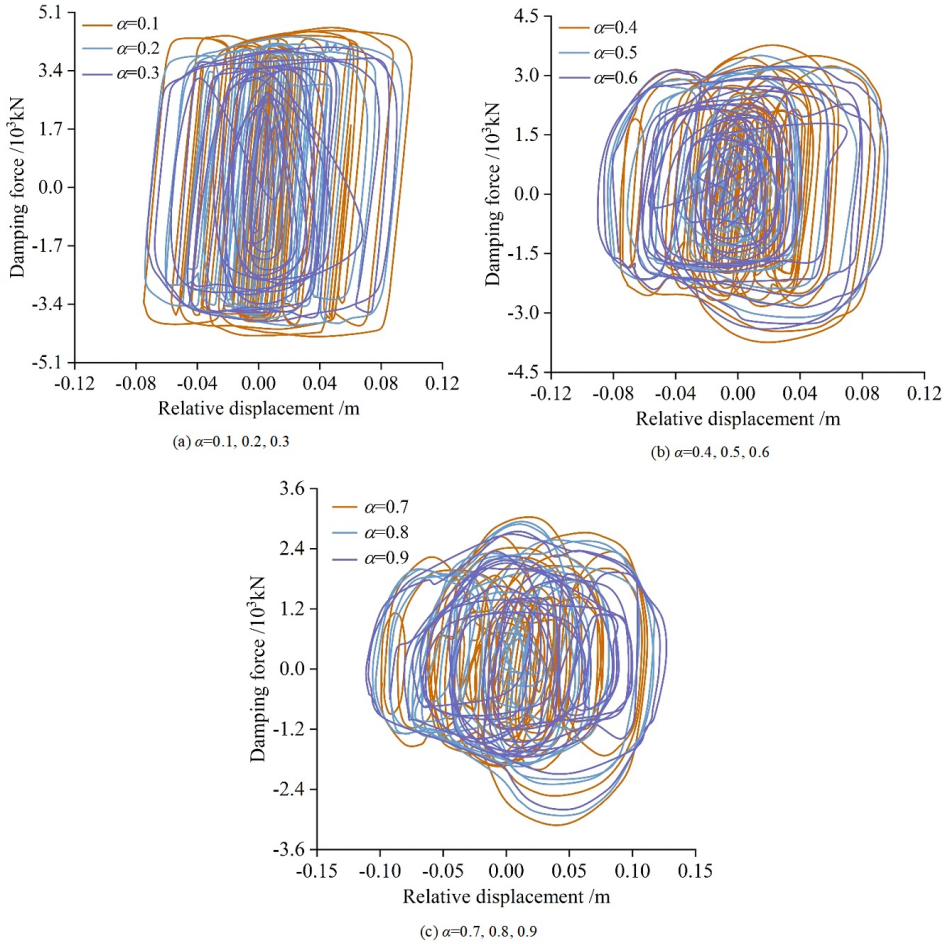

Figure 10: Energy dissipation curves of dampers under different speed index

4 Research on seismic response control and scheme optimization for high-rise buildings

This section verifies the effect of viscous dampers on the seismic response control of high-rise buildings based on actual engineering projects, proposes an optimized layout scheme for viscous dampers, and compares the seismic control effects of different arrangements.

4.1 Project overview

A high-rise building with a total of 47 floors, including 2 underground and 45 above-ground levels, has a total height of 146.61 meters. The structure adopts a reinforced concrete frame–core tube system. The first two floors feature a large podium structure, while the superstructure has a regular, bidirectionally symmetrical plan measuring 34 meters in length and 15.9 meters in width. For convenience, the two underground floors are taken as the starting point and numbered as floor 0.

4.1.1 Modal analysis

Modal analysis was performed using the Ritz vector method, and the modeling and calculations were carried out with ETABS software. The first three natural periods, frequencies, and mass participation coefficients of the structure are summarized in Table 1.

Table 1: First three modal parameters of the original structure

Modal	Dynamic parameters		Mass participation coefficient (%)		
	Period (s)	Frequency (Hz)	*UX*	*UY*	*RZ*
First mode	3.4352	0.3076	0	54	0
Second mode	2.7841	0.3825	58	0	1.9
Third mode	1.7468	0.6183	0.2	0	42

In the first mode, the Y-direction mass participation coefficient dominates, indicating translational vibration in the Y direction. In the second mode, the X-direction coefficient is 58%, indicating translational vibration in the X direction. In the third mode, the coefficient for rotation about the Z-axis reaches 42%, indicating noticeable torsional response. Since the building plan is relatively regular, the structure satisfies the requirements of reasonable conceptual seismic design.

4.1.2 Seismic analysis

The site is classified as a Type II site, with a design earthquake group of Group 2 and a seismic fortification intensity of 7 degrees. For time-history analysis, the peak acceleration of the selected seismic waves was scaled to 80 cm/s^2. Based on the site conditions and original spectrum analysis, the Taft wave, an artificial wave, and the Tangshan wave were selected. Considering bidirectional seismic input, the acceleration peak ratio was set to $X : Y = 1 : 0.82$.

Preliminary time-history calculations on the original structural model (without viscous dampers) were carried out using ETABS software. The results showed that under frequent earthquakes, the inter-story drifts in the X direction (20th–40th floors) and in the Y direction (20th–44th floors) exceeded allowable limits. To mitigate torsional effects, viscous dampers should be symmetrically arranged along the two main axes of the structure and uniformly distributed on floors with the largest inter-story drifts. This ensures that a relatively small number of dampers can achieve significant seismic control effects. Therefore, a bidirectionally symmetrical arrangement was adopted in both the X and Y directions, with a vertical continuous distribution from the 2nd to the 38th floors. The damper parameters were set as follows: damping coefficient $C = 3 \times 10^3\,\mathrm{kN \cdot s/m}$ and velocity index $\alpha = 0.4$.

4.2 Analysis of calculation results

4.2.1 Inter-story displacement angle and maximum horizontal displacement of floors

According to the "Code for Seismic Design of Buildings," under frequent seismic action, the maximum elastic inter-story drift angle of a frame–core wall structure should not exceed $1/800$. The inter-story drift angles of each floor and the maximum horizontal displacement of each floor for the original structure and the structure with viscous dampers (VD) are shown in Figures 11 and 12, respectively, before and after the installation of viscous dampers.

Since the overall stiffness of the structure in the X direction is significantly greater than that in the Y direction, under seismic loads, the maximum horizontal displacement and inter-story drift angle in the X direction are both smaller than those in the Y direction. Therefore, the influence of higher-order modes on the Y direction is more pronounced. Under frequent seismic loads, the original structure remains elastic. However, the results indicate that under Taft and Tangshan waves, the inter-story drift angle of some floors exceeds the limit value.

Compared to the original structure, the inter-story drift angles in the X direction for the VD structure decreased by an average of approximately 24.50%, 20.10%, and 15.64%, respectively, while those in the Y direction decreased by an average of approximately 13.50%, 15.71%, and 15.68%, respectively. Additionally, the maximum horizontal displacement of the floors also decreased accordingly, with the X direction decreasing by an average of approximately 28.50%, 20.15%, and 3.56%, respectively, and the Y direction decreasing by an average of approximately 13.31%, 28.11%, and 16.30%, respectively.

In summary, viscous dampers play a significant role in controlling the deformation of high-rise structures, substantially reducing the structural dynamic response, demonstrating notable vibration control effects, and ensuring structural safety.

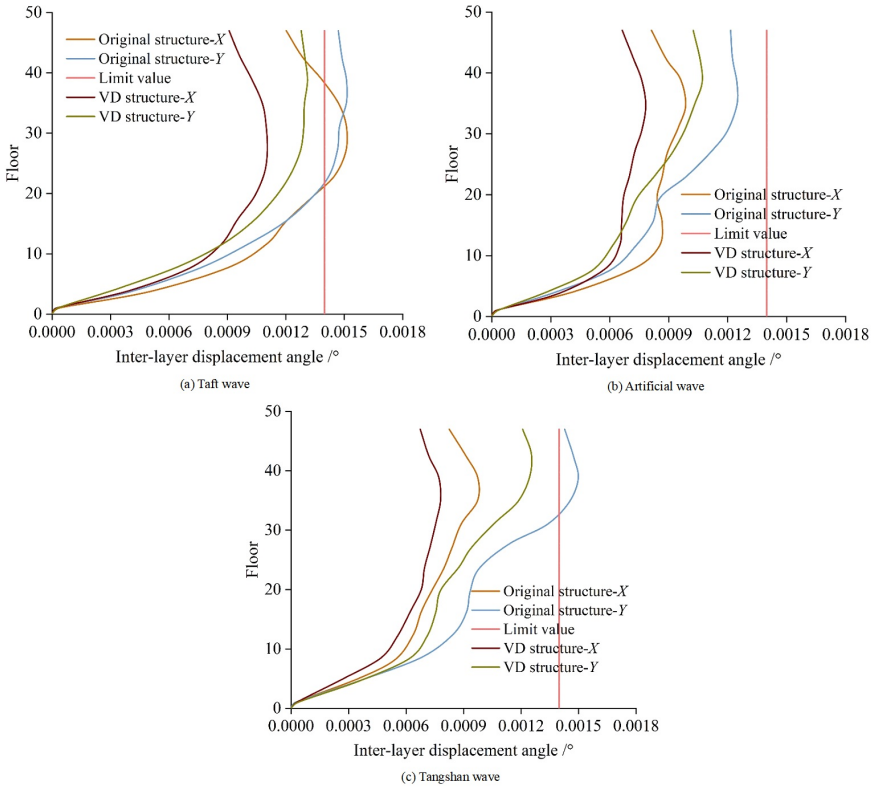

Figure 11: Comparison of inter-story displacement angles of structures under seismic action

4.2.2 Comparison of shear forces between structural layers

After installing viscous dampers, the structure acquires significant horizontal control forces, leading to notable reductions in inter-story shear forces. Under multiple earthquake actions, the comparison of inter-story shear force results for the original structure and the VD structure at each floor is shown in Figure 13. Subplots (a)–(f) represent: Taft wave–X direction, Taft

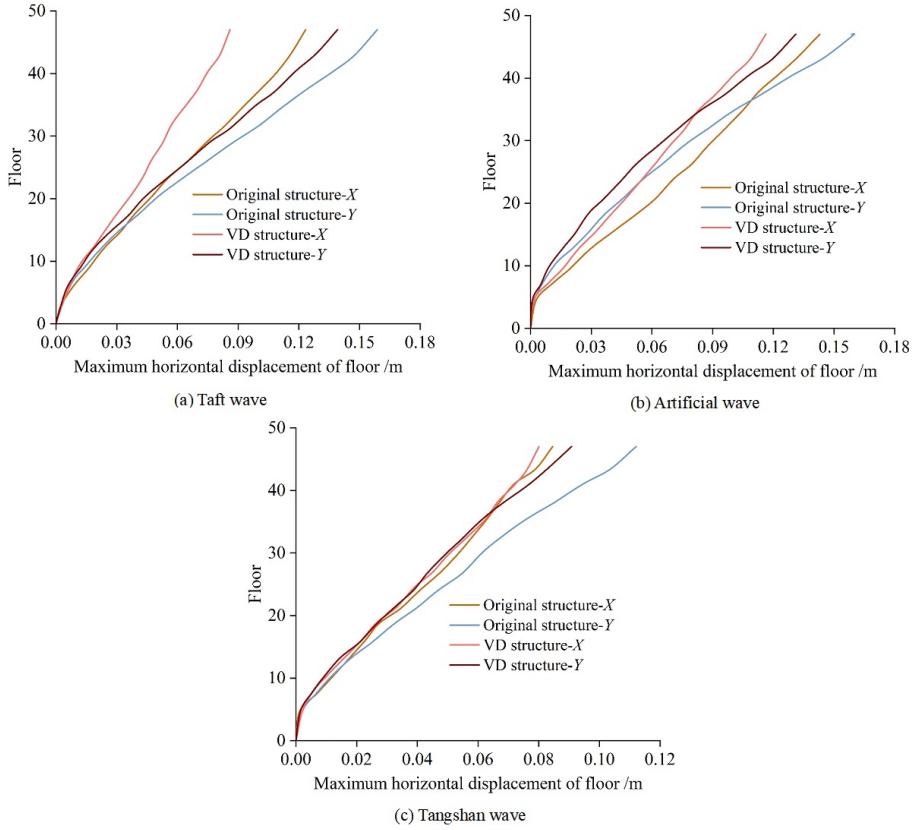

Figure 12: Comparison of the maximum horizontal displacement of structural floors

wave–Y direction, artificial wave–X direction, artificial wave–Y direction, Tangshan wave–X direction, and Tangshan wave–Y direction, respectively.

It can be observed that under the three types of seismic waves, the inter-story shear of the VD structure increases almost linearly from top to bottom, and the shear force of each floor in the VD structure generally remains within the range of the original structure. Specifically, the average reduction rates of inter-story shear in the X direction for the VD structure are 24.59%, 34.45%, and 9.81%, respectively, while the average reduction rates in the Y direction are 1.90%, 6.60%, and 8.65%, respectively. Among these, the reduction in base shear forces is particularly significant.

Additionally, under frequent earthquake loads, the installation of viscous dampers slightly increases the inter-story shear forces at certain floors in the Y direction. This occurs because, in practice, the stiffness of the viscous dampers and their support systems slightly increases the overall structural stiffness, preventing the idealized case of zero added stiffness. Since the reduction in inter-story displacement is not as significant as the increase in stiffness, a minor increase in inter-story shear is observed in those cases.

4.2.3 Energy response

Under multiple earthquake actions, most of the total seismic input energy is dissipated by structural modal damping, meaning that the structure itself bears the majority of the energy, resulting in a considerable seismic response. After adding viscous dampers, the dampers share part of this demand with the structural modal damping, dissipating energy jointly. The energy dissipation before and after structural control is summarized in Table 2.

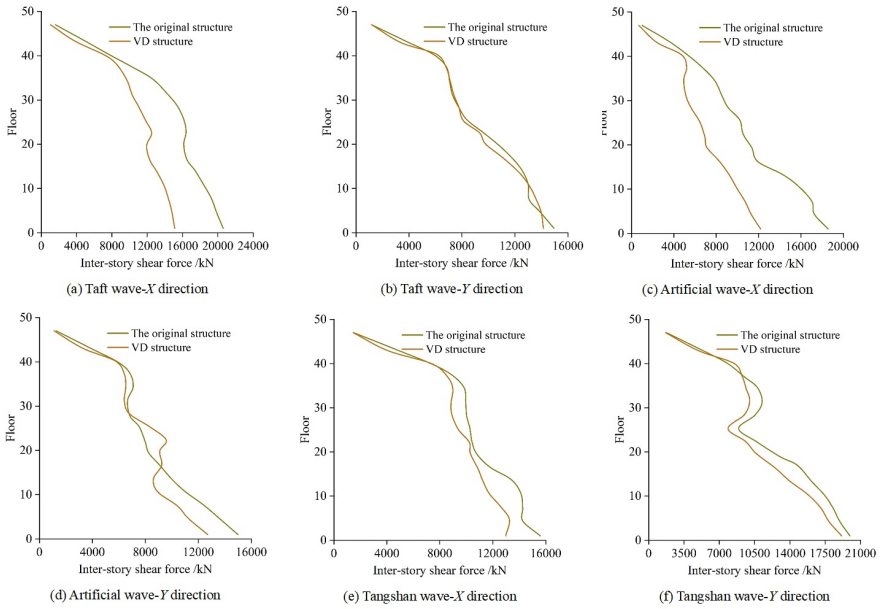

Figure 13: Comparison of the maximum inter-story shear force of structural floors

The results indicate that the proportion of energy dissipated by viscous dampers varies under different seismic inputs. Specifically, the energy dissipated by the dampers reached 35.05%, 35.06%, and 33.51% under the Taft, artificial, and Tangshan waves, respectively. These results demonstrate that viscous dampers play a crucial role in dissipating seismic input energy, substantially enhancing the safety and reliability of the structure. By relieving the structural system from absorbing the entire energy demand, viscous dampers improve both the performance and comfort of high-rise buildings under seismic conditions.

Table 2: Comparison of energy data before and after structural control

Structural type	Original structure			VD structure		
	Taft wave	Artificial wave	Tangshan wave	Taft wave	Artificial wave	Tangshan wave
Input energy /($\times 10^3$ kJ)	3.465	2.413	3.441	3.352	2.473	3.435
Modal damping energy dissipation /($\times 10^3$ kJ)	3.106	2.319	2.687	2.169	1.694	2.142
Damper energy dissipation /($\times 10^3$ kJ)	0	0	0	1.175	0.867	1.151
Energy dissipation ratio of damper	0	0	0	35.05%	35.06%	33.51%

4.3 Optimization of viscous damper layout

4.3.1 Scheme design

To determine the optimal damper placement, it is important to note that the control effect of viscous dampers is not limited to the stories where they are installed. Through the modal characteristics of the structure, the influence of dampers can extend throughout the entire building. Referring to inter-story displacement as the primary indicator, this study proposes five concentrated layout schemes and one alternate-story layout scheme, following principles such as installing dampers at floors with large inter-story displacements and minimizing the eccentricity between the center of mass and the center of rigidity. These schemes are evaluated with respect to their seismic mitigation effectiveness under different control objectives.

- **Option 1:** Viscous dampers continuously arranged at the lower part of the structure (floors 3–22).
- **Option 2:** Viscous dampers continuously arranged at the middle part of the structure (floors 12–32).
- **Option 3:** Viscous dampers continuously arranged at the upper part of the structure (floors 27–47).
- **Option 4:** Viscous dampers concentrated on floors with the largest inter-story deformations (floors 20–40).
- **Option 5:** Viscous dampers uniformly distributed at regular intervals across the structure, ensuring more balanced story yield coefficients and preventing localized concentration of inter-story displacements.

4.3.2 Structural vibration reduction scheme control comparison analysis

Based on the results of frequent and rare event time series analysis, the Taft wave, with its longer dominant period, is closer to the structure's natural vibration period and is more likely to cause resonance, resulting in the largest seismic response. Therefore, the Taft wave is used as the input seismic wave to investigate the structural response and seismic isolation effects under five schemes during frequent earthquakes.

The interstory drift angle comparisons are shown in Figure 14, with (a) and (b) representing the X-direction and Y-direction, respectively. It can be seen that all five schemes reduce the interstory drift angle to varying degrees, making it compliant with the seismic code specified limits. For Scheme 1, the reduction rates for inter-story displacement angles in the X and Y directions are 25.82% and 14.12%, respectively. For Scheme 2, they are 25.43% and 14.42%, respectively. For Scheme 3, they are 19.81% and 10.04%, respectively. For Scheme 4, they are 22.90% and 12.58%, respectively. For Scheme 5, they are 22.51% and 11.44%, respectively. Therefore, in terms of the reduction rate of inter-story displacement angle in the X direction, Schemes 1 and 2 are superior to the other schemes. In terms of the reduction rate of inter-story displacement angle in the Y direction, Scheme 2 is superior to the other schemes. Considering the inter-story displacement angle as the control target, Scheme 2 is the optimal choice.

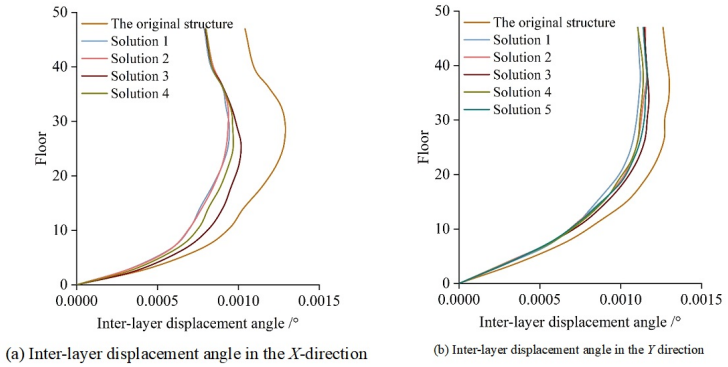

(a) Inter-layer displacement angle in the *X*-direction

(b) Inter-layer displacement angle in the *Y* direction

Figure 14: Five layout schemes for inter-floor displacement angles

For Schemes 1 to 5, the peak horizontal displacement in the X-direction at the top node decreased from 0.1364 m to 0.0835 m, 0.0804 m, 0.0961 m, 0.0820 m, and 0.0876 m, respectively,

with vibration reduction rates of 38.78%, 41.06%, 29.55%, 39.88%, and 35.78%, respectively. In the Y-direction, the peak horizontal displacements decreased from 0.1514 m to 0.1373 m, 0.1329 m, 0.1365 m, 0.1347 m, and 0.1362 m, respectively, with vibration reduction rates of 9.31%, 12.22%, 9.84%, 11.03%, and 10.04%, respectively. In terms of vibration reduction rates in the X and Y directions, Scheme 2 is slightly superior to the other schemes. Therefore, when using the peak displacement response at the top-floor nodes as the control target, Scheme 2 is more advantageous. Whether considering inter-story displacement or top-floor peak displacement, for displacement control purposes, installing viscous dampers on lower floors is more advantageous. Schemes 1 and 2 are installed at lower floors, but Scheme 2 has better control performance than Scheme 1, indicating that lower is not necessarily better, which is related to the deformation characteristics of the structural type. In frame-shear wall structures, lateral displacement deformation exhibits a "bending-shearing" pattern, with smaller deformation at the lower part. Scheme 1 is installed too low, resulting in smaller structural deformation, which is unfavorable for the functionality of the dampers. Therefore, installing them at the middle floors of the structure is relatively better.

The peak acceleration responses of the top-most node for different schemes are shown in Table 3. It can be seen that viscous dampers significantly reduce the acceleration response of the top-most node under seismic loads. Regarding the reduction rate of peak acceleration at the top-level node in the X-direction, Scheme 1 achieves 18.29%, slightly better than other schemes. In the Y-direction, Scheme 4 achieves a reduction rate of 15.09%, outperforming Schemes 3 and 5, and far superior to Schemes 1 and 2. In summary, Scheme 4 achieves a peak acceleration reduction rate exceeding 15% in both the X and Y directions, slightly outperforming Scheme 5 and significantly outperforming Schemes 1, 2, and 3. Therefore, when the peak acceleration response of the top-level nodes is the control objective, Scheme 4, which positions the viscous dampers at the locations with the largest actual inter-story deformations, is the optimal solution.

Table 3: Horizontal peak acceleration response of top-level nodes in the structure

Name of the plan	X direction /m·s^{-2}	Reduction rate /%	Y direction /m·s^{-2}	Reduction rate /%
The original structure	1.624	0	1.359	0
Solution 1	1.327	18.29	1.295	4.71
Solution 2	1.354	16.63	1.247	8.24
Solution 3	1.462	9.98	1.158	14.79
Solution 4	1.376	15.27	1.154	15.09
Solution 5	1.383	14.84	1.157	14.86

5 Conclusion

This study examined the influence of viscous damper parameters on the seismic response control of high-rise buildings using the Maxwell model and validated the findings through engineering examples to optimize damper layouts. The following conclusions are drawn:

The maximum horizontal displacement of floors and the seismic reduction rate of inter-story shear generally increase monotonically with the damping coefficient. Under varying damping parameter conditions, the maximum reduction rates for horizontal displacement and inter-story shear reached 73.68% and 37.04%, respectively. The displacement reduction effect was more pronounced than shear reduction, indicating that viscous dampers are more effective in controlling horizontal displacement than inter-story shear, and that the damping coefficient has a

significant impact on performance.

As the velocity index increases, the area enclosed by the energy dissipation curves remains nearly unchanged, demonstrating that the velocity index has negligible influence on the hysteresis loop area. From the perspective of the energy dissipation mechanism of viscous dampers, its effect on energy dissipation capacity is minimal.

Under frequent seismic loads, the performance of the VD structure is substantially superior to that of the original structure. The inter-story displacement angles decrease significantly, with a maximum reduction of 24.50%. The maximum horizontal floor displacement decreases by more than one-quarter, confirming the strong seismic response control and damping effectiveness of viscous dampers.

When peak acceleration at the top node is the control objective, Option 4 proves optimal, with a reduction rate exceeding 15%. When inter-story drift angle is the objective, Option 2 performs best, achieving a reduction rate of 25.43%. For top-floor peak displacement, Option 2 again shows outstanding performance, with a reduction rate as high as 41.06%.

Considering engineering practice and structural functional requirements, damper arrangement should be determined by selecting appropriate structural response indices as control objectives. Combining the results of actual seismic response analysis with the structural characteristics of lateral displacement makes it possible to achieve tailored, project-specific solutions and obtain optimal damping effects.

References

[1] Mrad, C., Titirla, M. D., & Larbi, W. (2021). Comparison of strengthening solutions with optimized passive energy dissipation systems in symmetric buildings. *Applied Sciences, 11*(21), 10103.

[2] Titirla, M. D. (2023). A state-of-the-art review of passive energy dissipation systems in steel braces. *Buildings, 13*(4), 851.

[3] Nurchasanah, Y., & Harnadi, M. L. (2021, April). Assessment of viscous damper placement as passive energy dissipation on high-rise building, a numerical study. In *Journal of Physics: Conference Series* (Vol. 1858, No. 1, p. 012096). IOP Publishing.

[4] Almajhali, K. Y. M. (2023, May). Review on passive energy dissipation devices and techniques of installation for high rise building structures. In *Structures* (Vol. 51, pp. 1019-1029). Elsevier.

[5] Bagheri, S., & Rahmani-Dabbagh, V. (2018). Seismic response control with inelastic tuned mass dampers. *Engineering Structures, 172*, 712-722.

[6] Salvi, J., & Rizzi, E. (2015). Optimum tuning of Tuned Mass Dampers for frame structures under earthquake excitation. *Structural Control and Health Monitoring, 22*(4), 707-725.

[7] Vellar, L. S., Ontiveros-Pérez, S. P., Miguel, L. F. F., & Fadel Miguel, L. F. (2019). Robust optimum design of multiple tuned mass dampers for vibration control in buildings subjected to seismic excitation. *Shock and Vibration, 2019*(1), 9273714.

[8] Das, S., & Choudhury, S. (2017). Seismic response control by tuned liquid dampers for low-rise RC frame buildings. *Australian Journal of Structural Engineering, 18*(2), 135-145.

[9] Kang, X., Tang, J., Li, F., Wu, J., Wei, J., Huang, Q., ... & Sheng, Z. (2023). Optimal tuned inerter dampers for vibration control performance of adjacent building structures. *Buildings, 13*(7), 1803.

[10] Tang, Z., Sheng, J., & Dong, Y. (2023). Effects of tuned liquid dampers on the nonlinear seismic responses of high-rise structures using real-time hybrid simulations. *Journal of Building Engineering, 70*, 106333.

[11] Wang, Q., Qiao, H., De Domenico, D., Zhu, Z., & Tang, Y. (2020). Seismic response control of adjacent high-rise buildings linked by the Tuned Liquid Column Damper-Inerter (TLCDI). *Engineering Structures, 223*, 111169.

[12] Elias, S., Rupakhety, R., & Ólafsson, S. (2020). Tuned mass dampers for response reduction of a reinforced concrete chimney under near-fault pulse-like ground motions. *Frontiers in Built Environment, 6*, 92.

[13] Radmard Rahmani, H., & Könke, C. (2019). Seismic control of tall buildings using distributed multiple tuned mass dampers. *Advances in Civil Engineering, 2019*(1), 6480384.

[14] Abd-Elhamed, A., & Tolan, M. (2022). Tuned liquid damper for vibration mitigation of seismic-excited structures on soft soil. *Alexandria Engineering Journal, 61*(12), 9583-9599.

[15] Rozas, L., Boroschek, R. L., Tamburrino, A., & Rojas, M. (2016). A bidirectional tuned liquid column damper for reducing the seismic response of buildings. *Structural Control and Health Monitoring, 23*(4), 621-640.

[16] Zhu, R., Guo, T., & Mwangilwa, F. (2020). Development and test of a self-centering fluidic viscous damper. *Advances in Structural Engineering, 23*(13), 2835-2849.

[17] Sabino, A., Mannella, A., & de Leo, A. M. (2020). Seismic response of a structure equipped with an external viscous damping system. *Buildings, 10*(2), 19.

[18] Javadinasab Hormozabad, S., & Zahrai, S. M. (2019). Innovative adaptive viscous damper to improve seismic control of structures. *Journal of Vibration and Control, 25*(12), 1833-1851.

[19] Zand, H., & Akbari, J. (2018). Selection of viscous damping model for evaluation of seismic responses of buildings. *KSCE Journal of Civil Engineering, 22*(11), 4414-4421.

[20] Yaghmaei-Sabegh, S., Jafari-Koucheh, E., & Ebrahimi-Aghabagher, M. (2020, December). Estimating the seismic response of nonlinear structures equipped with nonlinear viscous damper subjected to pulse-like ground records. In *Structures* (Vol. 28, pp. 1915-1923). Elsevier.

[21] Kookalani, S., & Shen, D. (2020). Effect of Fluid Viscous Damper parameters on the seismic performance. *Journal of Civil Engineering and Materials Application, 4*(3), 141-153.

[22] Deringöl, A. H., & Güneyisi, E. M. (2021, December). Influence of nonlinear fluid viscous dampers in controlling the seismic response of the base-isolated buildings. In *Structures* (Vol. 34, pp. 1923-1941). Elsevier.

[23] Wolff, E. D., Ipek, C., Constantinou, M. C., & Tapan, M. (2015). Effect of viscous damping devices on the response of seismically isolated structures. *Earthquake Engineering & Structural Dynamics, 44*(2), 185-198.

[24] Ras, A., & Boumechra, N. (2016). Seismic energy dissipation study of linear fluid viscous dampers in steel structure design. *Alexandria Engineering Journal, 55*(3), 2821-2832.

[25] Tan, L., Lu, L., Tang, G. Q., Cheng, L., & Chen, X. B. (2019). A viscous damping model for piston mode resonance. *Journal of Fluid Mechanics, 871*, 510-533.

[26] Milanchian, R., Hosseini, M., & Nekooei, M. (2020). Vertical isolation of 1-story structures with the nonlinear viscous dampers for seismic response reduction. *Journal of Civil and Environmental Engineering, 50*(98), 65-76.

[27] De Domenico, D., Ricciardi, G., & Takewaki, I. (2019). Design strategies of viscous dampers for seismic protection of building structures: a review. *Soil Dynamics and Earthquake Engineering, 118*, 144-165.

[28] Dall'Asta, A., Scozzese, F., Ragni, L., & Tubaldi, E. (2017). Effect of the damper property variability on the seismic reliability of linear systems equipped with viscous dampers. *Bulletin of Earthquake Engineering, 15*(11), 5025-5053.

[29] Del Gobbo, G. M., Williams, M. S., & Blakeborough, A. (2018). Comparing fluid viscous damper placement methods considering total-building seismic performance. *Earthquake Engineering & Structural Dynamics, 47*(14), 2864-2886.

[30] Chen, X., & Xiong, J. (2022). Seismic resilient design with base isolation device using friction pendulum bearing and viscous damper. *Soil Dynamics and Earthquake Engineering, 153*, 107073.

[31] Cucuzza, R., Domaneschi, M., Greco, R., & Marano, G. C. (2023). Numerical models comparison for fluid-viscous dampers: performance investigations through genetic algorithm. *Computers & Structures, 288*, 107122.

[32] Kandemir-Mazanoglu, E. C., & Mazanoglu, K. (2017). An optimization study for viscous dampers between adjacent buildings. *Mechanical Systems and Signal Processing, 89*, 88-96.

[33] VVasile, O., & Bugaru, M. (2022). A new modeling approach for viscous dampers using an extended Kelvin–Voigt rheological model based on the identification of the constitutive law's parameters. *Computation, 11*(1), 3.

[34] Chalarca, B., Filiatrault, A., & Perrone, D. (2022, September). Parametric study and prediction models of the seismic response of single-degree-of-freedom structural systems equipped with Maxwell material fluid viscous dampers. In *Structures* (Vol. 43, pp. 388-406). Elsevier.

[35] Liu, W., Ikago, K., Wu, Z., & Fukuda, I. (2022). Modified tuned Maxwell–Wiechert model for improving seismic performance of base-isolated structures. *Journal of Building Engineering, 54*, 104616.